WILEY | Hindawi

Research Article

Permeability Characterization and Its Correlation with Pore Microstructure of Stress-Sensitive Tight Sandstone: Take Chang 6 in Ordos Basin for Example

Yilin Chang [1,2,3] **Zhengming Yang,**[2,3] **Yapu Zhang** [2,3] **Zhongkun Niu** [1,2,3] **and Xinliang Chen**[1,2,3]

[1]*University of Chinese Academy of Sciences, Beijing 100049, China*
[2]*Institute of Porous Flow and Fluid Mechanics, Chinese Academy of Sciences, Langfang, Hebei 065007, China*
[3]*Department of Porous Flow & Fluid Mechanics, Research Institute of Petroleum Exploration & Development, PetroChina Company Limited, Langfang, Hebei 065007, China*

Correspondence should be addressed to Yilin Chang; changyilin21@mails.ucas.ac.cn

Tight reservoirs are sensitive to stress changes during fracturing and oil and gas production. Facing different production modes, the variation characteristics of rock permeability and pore structure need to be further clarified. In this study, using a self-built high temperature and pressure physical simulation device and NMR equipment, the influence of the stress loading method, cyclic loading, and loading rate on rock permeability and pore characteristics were analyzed, and the relationship between them was clarified. The permeability sensitivity under variable confining pressure (63.3%) was greater than that of variable flow pressure (46.4%). The damage rate decreased with repeated loading (63.3%-35.8%) and increased loading rate (53.1%-42.3%). As for the pore features, when the net stress increased, the volume variation range of micropores was greater than that of mesopores. The damage rate of permeability (63.3%) was obviously larger than that of pore volume (10.4%). The slope of the fitted curve of permeability and pore volume decreased evidently with loading times. The structure deformation of rock skeleton and the migration of cement had a great influence on permeability in the first loading. Later, it was mainly the bulk deformation of rock particles, the particles' contact surface increasing and the seepage space shrinking slowly. Eventually, the permeability remained stable due to the limited pore compression. This study can provide a reference for designing reasonable production parameters and reducing formation damage.

1. Introduction

As a considerable part of unconventional energy, tight oil resources are abundant and widely distributed, making it a new hot spot for global oil exploration and development [1–3]. The Chang 6 reservoir, an important exploration target in the Ordos Basin, is a typical tight oil reservoir, which is characterized by poor physical properties and strong heterogeneity [4–6]. The matrix permeability is generally less than 0.1 mD and porosity is less than 10%, which shows obvious stress-sensitive features [7, 8]. To realize the industrialized exploitation of tight oil, the formation is generally reformed through staged fracturing and other engineering

[9, 10]. Considering the whole production process, the pressure on formation rocks is in dynamic change. During fracturing, the pressure increases rapidly until fractures are formed. With the extraction of crude oil, the flow pressure gradually decreases, the net stress on the rock increases, and the rock permeability decreases, a large amount of fluid is trapped in the micronanopore and throat, affecting the ultimate recovery [11–13]. It is necessary to investigate the influence of pressure change on porosity and permeability of formation rock in different stages of production process [14, 15].

Researchers have carried out related research on the change of permeability with net stress for different blocks

and different types of rocks [16–20]. The stress sensitivities of rocks were evaluated by various methods, such as the industry-standard method and the stress sensitivity coefficient method [21, 22]. At the same time, fitting the permeability-net stress change with a function, the empirical formula of permeability change with net stress was obtained and the corresponding mathematical model was established [23, 24]. In addition, the influencing factors of the stress-sensitive characteristics of rocks were analyzed, mainly including the properties of the rock itself (such as pore structure, mineral composition, and cementation characteristics) and external environmental factors (such as the state of rock stress and temperature) [25–29]. The main reason for the permeability change under different stress is the deformation of porous media, which is usually divided into bulk deformation and structural deformation [30–33]. Bulk deformation refers to the shrinkage of the volume of rock particles under compression, whereas the relative spatial position of the particles does not alter. Structural deformation means that the arrangement and relative position of particles change. Bulk deformation is generally regarded as elastic or elastic-plastic deformation, while structural deformation is plastic deformation, with a low possibility of recovery.

When the rock is compressed, its pore structure changes, throat narrows, seepage space shrinks, and permeability decreases, forming stress sensitivity damage [34–37]. The stress sensitivity study mainly focuses on the change of core permeability, but it lacks the description of pore throat structure characteristics, especially under different stress conditions. Low-field NMR technology can accurately catch internal pore and throat characteristics in tight cores. Combined with online displacement, the variation features of pores with different sizes can be obtained under different working conditions [38–40].

In this study, the tight sandstone of Chang 6 reservoir was taken as an example to investigate the influence of loading method, cyclic loading, and loading rate on its permeability. Combined with low-field NMR online displacement technology, the variation characteristics of pores microstructures under different working conditions were obtained, which contributes to clarifying the internal mechanism of permeability changes. Finally, a theoretical reference is provided for reasonably setting up production parameters and reducing reservoir damage.

2. Experimental Section

2.1. Experimental Materials. The core samples were obtained from Chang 6 reservoir of Triassic Yanchang Formation in Ordos Basin. The basic physical parameters and mineral composition of core samples are shown in Tables 1 and 2, respectively. The average porosity of the rock sample is 12.35%, the average permeability is 0.25 mD, and the main mineral components are quartz and feldspar.

The fluid used in this study was brine with a total salinity of 23003 mg/L. Its components include $NaHCO_3$, Na_2SO_4, $CaCl_2$, $MgCl_2$, NaCl, and KCl (Sinopharm Chemical Reagent Co., Ltd., Shanghai, China) and its ion content is shown in Table 3.

2.2. Equipment and Procedure. Nuclear magnetic resonance (NMR) is used to detect the pore structure of rock by measuring the amplitude and relaxation rate of the NMR relaxation signal of the hydrogen nucleus in the rock pore fluid [41, 42]. When single-phase fluid is satisfied and the echo interval of CPMG sequence is short enough, the transverse relaxation rate of NMR in porous media can be approximately written as

$$\frac{1}{T_2} \approx \frac{1}{T_{2\text{surface}}} = \rho_2 \frac{S}{V}, \tag{1}$$

where T_2 is the transverse relaxation time, $T_{2\text{surface}}$ is the surface relaxation time, ρ_2 is the transverse surface relaxation strength, S/V is the surface to volume ratio of the examined core samples. This equation describes the relationship between relaxation time and surface to volume ratio, which can be used to divide pore size. The T_2 spectrum area reflects the pore size. When it changes, it means that the pore size and structure change.

The experiments were mainly divided into two parts. Firstly, a self-built physical simulation device was used to measure permeability under different net stress. Then, the low-field NMR online analysis system (MacroMR12-150H, Suzhou Niumag Analytical Instruments Co., Ltd., Suzhou, China) was utilized to study the variation of pore volume under the same conditions. The experimental parameters and device diagram are shown in Table 4 and Figure 1.

(1) The cores were cut, put into the ultrasonic cleaning instrument for 1 min, and put into the oven at 100°C for 8 h. Then, a vacuum saturation device was used to saturate the core with salinity water. (2) Put the core into the holder and connect the salinity water at the inlet, and the experimental temperature was 70°C. (3) Variable confining pressure operation: the outlet of the holder was connected to the atmosphere. The net stress was adjusted by increasing confining pressure to 2.5, 5, 8, 11, 15, 20, and 30 MPa, respectively. The salinity water was injected into the core at a rate of 0.1 mL/min. When the net stress reached 30 MPa, reduce the pressure according to 20, 15, 11, 8, 5, and 2.5 MPa. Each pressure point lasts 40-60 min during loading and 60-90 min during unloading. (4) Variable flow pressure operation: the outlet of the holder was connected to the back pressure valve. Reduce the backpressure to adjust the net stress, whose setting was the same as the variable confining pressure. (5) At each net stress, the steady inlet pressure was recorded and the core permeability was calculated by Darcy's formula [43]

$$\sigma_{\text{net}} = P_c - P_p = P_c - \frac{(P_{\text{in}} + P_{\text{out}})}{2}, \tag{2}$$

where σ_{net} is the net stress, MPa [44]; P_c is the confining pressure, MPa; P_P is flow pressure, MPa; P_{in} is the pressure of holder inlet, MPa; P_{out} is the pressure of holder outlet, MPa.

$$k = \frac{20Q\mu L}{3\pi d^2 \Delta p}. \tag{3}$$

TABLE 1: Parameters of core samples.

Serial number	Length/mm	Diameter/mm	Porosity/%	Permeability/mD
1	49.94	25.30	11.13	0.28
2	48.09	25.37	12.32	0.32
3	50.85	25.45	12.78	0.31
4	49.58	25.34	12.02	0.26
5	50.33	25.34	13.17	0.21
6	49.17	25.37	12.98	0.28
7	48.93	25.36	11.74	0.32
8	49.21	25.25	12.92	0.15
9	48.36	25.37	12.54	0.24
10	49.56	27.37	11.89	0.25

TABLE 2: The mineral composition of cores.

Component	Quartz	Potassium feldspar	Plagioclase	Calcite	Clay minerals
Proportion/%	50	6	21	14	9

TABLE 3: Composition of the formation brine.

Ions	Na^+	K^+	Ca^{2+}	Mg^{2+}	HCO_3^-	SO_4^{2-}	Cl^-
Concentration/($mg \cdot L^{-1}$)	8563	94	209	52	1486	1800	10799

TABLE 4: Different net stress change modes and their correspondence with actual working conditions.

Modes		Net stress/MPa	Corresponding working conditions
Loading method	Variable confining pressure	2.5-5-8-11-15-20-30-20-15-11-8-5-2.5	Overburden pressure change
	Variable flow pressure	2.5-5-8-11-15-20-30-20-15-11-8-5-2.5	Reservoir fluid-producing
Cyclic loading		2.5-5-8-11-15-20-30-20-15-11-8-5-2.5-5-8-11-15-20-30-20-15-11-8-5-2.5	Energy supplement-production process
Loading rate		2.5-5-7.5-10-12.5-15-17.5-20-30 2.5-5-10-15-20-30 2.5-10-20-30	Different oil production rate

where k is permeability, mD; Q is flow, mL/min; μ is fluid viscosity, MPa·s; L is core length, cm; d is core diameter, cm; Δp is the pressure difference across the core, MPa.

When analyzing pore variation characteristics, (1) turn on the heating device and set the holder temperature to 70°C and ensure the temperature of the test coil was 32°C. (2) Calibrate NMR instruments and acquire substrate signals. (3) Repeat the above steps to adjust net stress and test the T_2 curve to obtain the volume change of the different sizes pores under each net stress.

3. Results and Discussion

Combined with the actual production condition in the field, this study analyzed the effects of stress loading methods,

cyclic loading, and different loading rates on rock permeability and pore features, and clarified the correlation between them.

$$E_s = \frac{k_0 - k_i}{k_0},$$
$$E_h = \frac{k_{ui}}{k_i}, \tag{4}$$

where E_s is the permeability damage rate; E_h is the permeability recovery rate; k_i is the permeability under different net stress during loading, mD; k_0 is the permeability at the initial 2.5 MPa, mD; k_{ui} is the permeability under different net stress during unloading, mD.
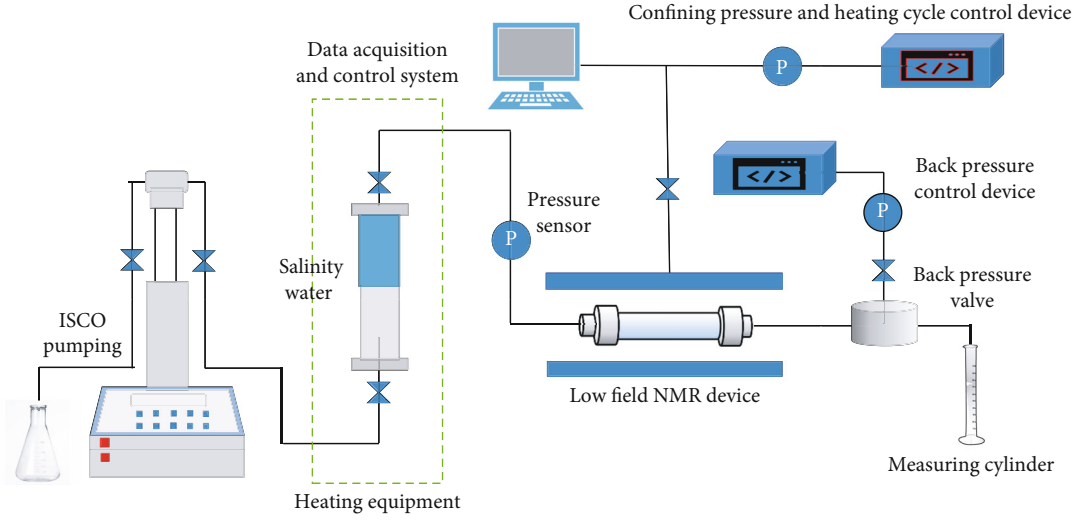
FIGURE 1: Schematic diagram of the experimental device.

$$R_s = \frac{A_0 - A_i}{A_0},$$
$$R_h = \frac{A_{ui}}{A_i}, \tag{5}$$

where R_s is the porosity damage rate; R_h is the porosity recovery rate; A_i is the peak area of T_2 spectrum under different net stress during loading, A_0 is the peak area at 2.5 MPa; A_{ui} is the peak area of T_2 spectrum under different net stress during unloading.

3.1. Effect of Net Stress on Permeability

3.1.1. Loading Method.
There are two methods for measuring stress sensitivity, variable confining pressure and variable flow pressure. The former experimental device is simple and easy to operate, while the latter is more in line with the pressure changes in the actual production process. The influence of the two loading methods on permeability will be analyzed in this section.

As shown in Figure 2(a), when the net stress increases with the change of confining pressure, the permeability decreases rapidly. The turning point is around 8 MPa, beyond which the change of permeability slows down and then gradually stabilizes, indicating that the compression of the core skeleton has a certain limit. The permeability recovers slowly during the unloading process. Similarly, the permeability recovers quickly before the critical point, but cannot return to the initial state. Figure 2(b) depicts the damage rate and recovery rate of permeability under different net stress. The initial change rate is relatively fast. The damage rate reaches 55.1% at 8 MPa and the final damage rate is 63.3%, meaning that the later stress changes have little effect on permeability. With the increase of net stress, the recovery rate gradually increases, ranging from 54.7% to 94.5%. After 8 MPa, the recovery rate remains almost unchanged, all exceeding 95%. It illustrates that the permeability changes obviously and is difficult to recover at

the initial stage of loading, which is the main permeability damage region.

Figure 3 demonstrates the relationship between permeability and net stress by adjusting the flow pressure. Likewise, permeability decreases with increasing net stress. The initial decline rate is slightly faster, the overall decline rate is relatively uniform. The final permeability damage rate is 46.4%, lower than that of variable confining pressure. In terms of recovery rate, there is also an irrecoverable section in the variable flow pressure test. Except that the recovery rate is 83.3% at 2.5 MPa, the others are more than 90%. In this study, the net stress is calculated according to the classical Terzaghi method, in which the effective stress coefficient is regarded as 1. However, the effective stress coefficient of tight sandstone is less than 1, so the net stress of rock under variable flow pressure is less than the variable confining pressure. Correspondingly, the permeability damage rate is lower.

3.1.2. Cyclic Loading.
The formation pressure decreases gradually during the production process. By some energy supplement measures, such as shut-in for energy storage or water injection, the pressure will recover slowly. There is a dynamic change of increase-decrease in the net stress on the rock. To clarify the influence of this cyclic on permeability, repeated core loading and unloading experiments have been done.

Figure 4(a) illustrates that during the second loading, although the changing trend of permeability is the same as the first time, fast followed by slow, the amount of change is significantly reduced. Figures 4(b) and 4(c) show the damage rate and recovery rate of core permeability during cycling. The final permeability damage rate of the first loading (63.3%) is much higher than that of the second loading (35.8%). After repeated loading, the stress sensitivity turns moderately weak. As for the recovery rate, during the initial loading, the recovery rate increases with net stress and gradually remains unchanged exceeding the critical stress. While the secondary recovery rate has no marked change and maintains a high level, with a minimum value of 94.4%. It
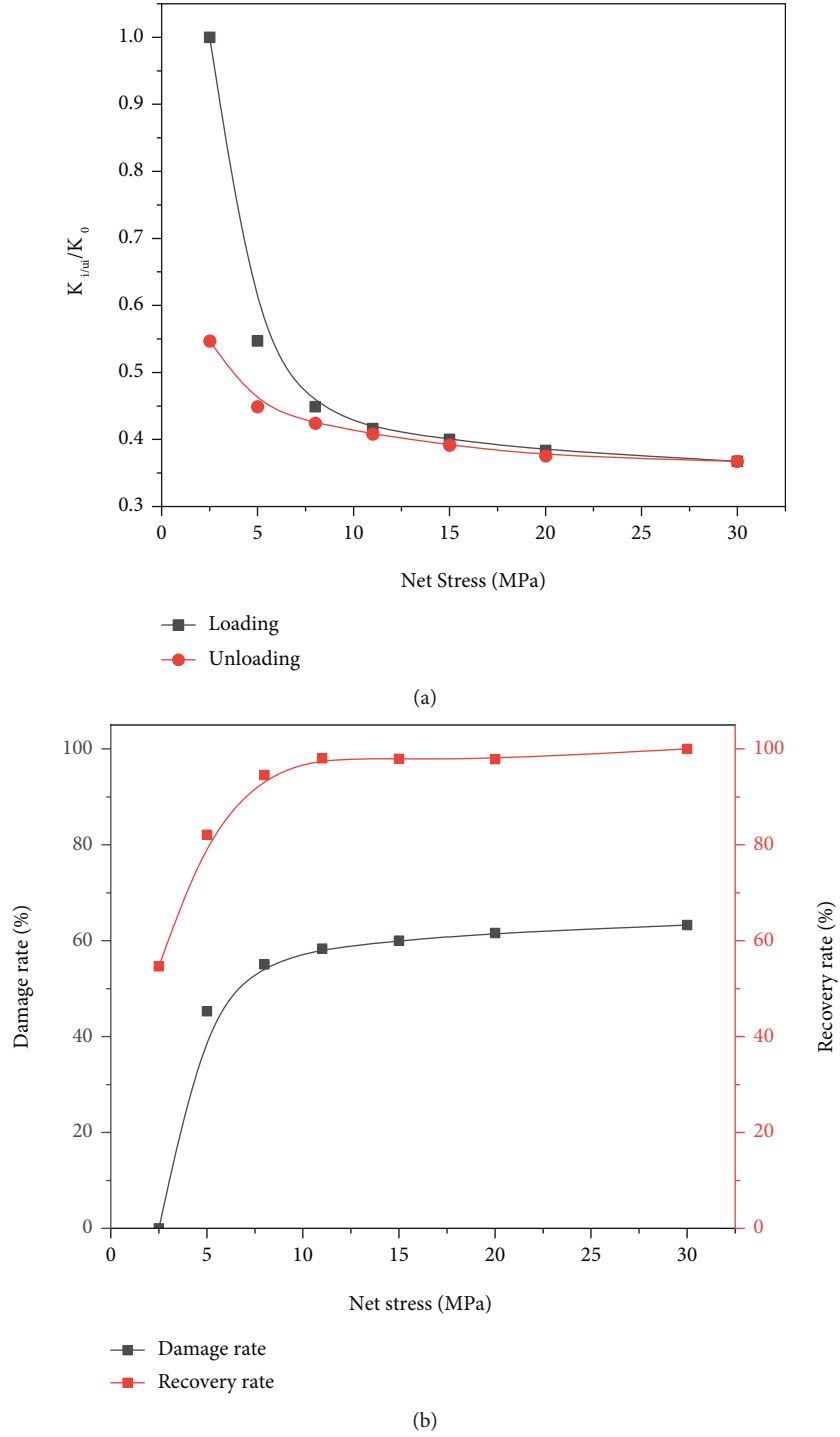
(a)

(b)

FIGURE 2: Variable confining pressure: (a) the relation between dimensionless permeability and net stress; (b) permeability damage and recovery rate under different net stress.

indicates that after the initial loading, the overall structure of the core is stable and the elastic deformation increases, thus the permeability is easy to recover.

3.1.3. Loading Rate. Different oil production rates are set in the production process, resulting in different change rates of flow pressure. In this section, the net stress loading rate was adjusted at the rates of 2.5, 5, and 10 MPa/h, respec-

tively, which helps to clarify the influence of the change rate of the net stress on the permeability.

It can be seen from Figure 5 that with the increase of loading rate, the variation of permeability decreases, ranging from 53.1% to 42.3%. Under the loading rate of 2.5 MPa/h and 5 MPa/h, the stress sensitivity damage rate is close, and the stress sensitivity degree is moderately strong. However, when the loading rate is set to 10 MPa/h, the damage
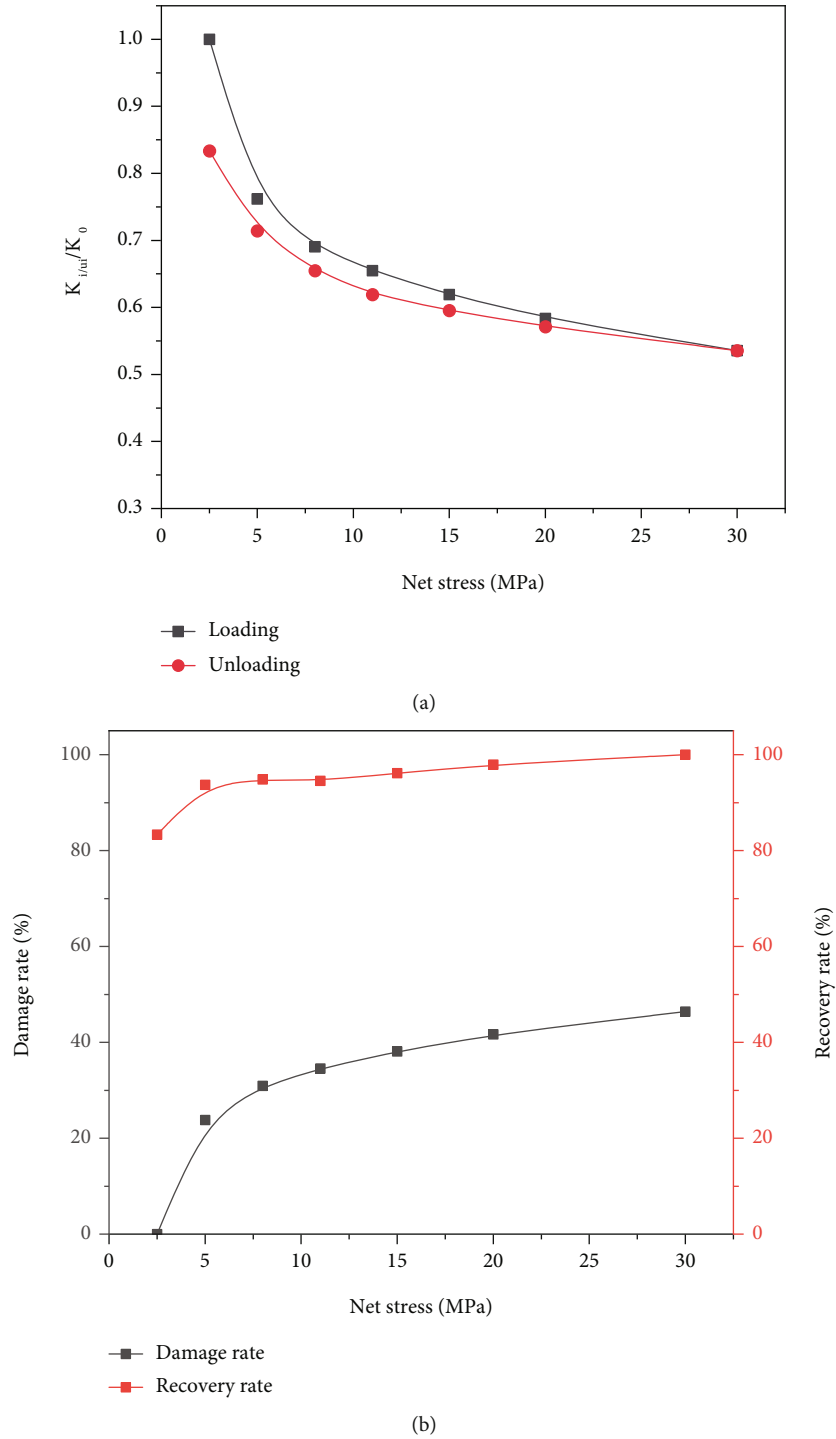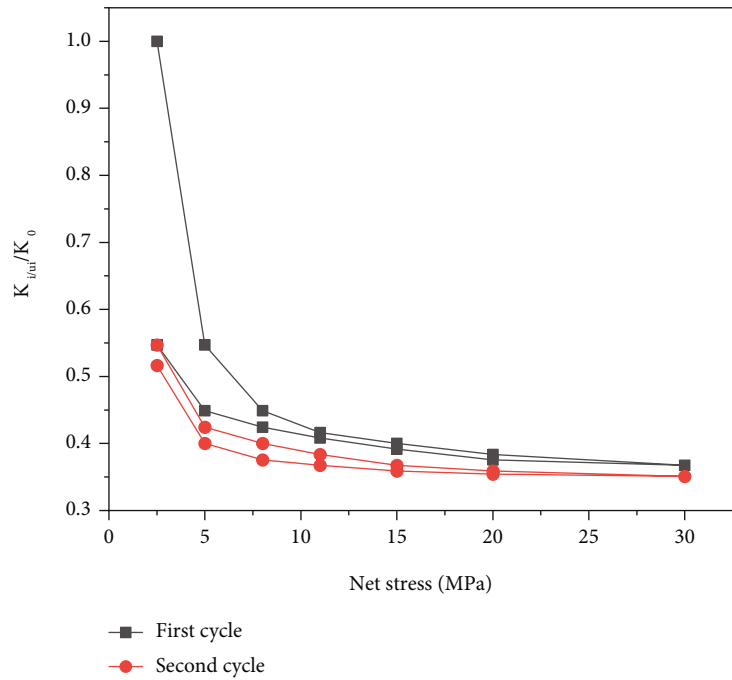
(a)

(b)

FIGURE 3: Variable flow pressure: (a) the relation between dimensionless permeability and net stress; (b) permeability damage and recovery rate under different net stress.

rate is the smallest and the stress sensitivity is moderately weak. Before the critical stress, the permeability decreased rapidly with the increase of the net stress. When the core is compressed, the particles near the larger pore throat first slip and deform, resulting in a great decrease in permeability. The particles around the micropores are closely arranged and stable and the stress needs to be conducted gradually. The longer the loading time, the more obvious shrinkage

of the pore space, and the greater impact on the pore throat structure.

3.2. Effect of Net Stress on Pore Characteristics with LF-NMR.
The low-field NMR device can be used to obtain the T_2 spectrum of the core saturated with salinity water. By collecting the T_2 spectrum of cores under different net stress and counting the peak areas, the volumes of pores of different
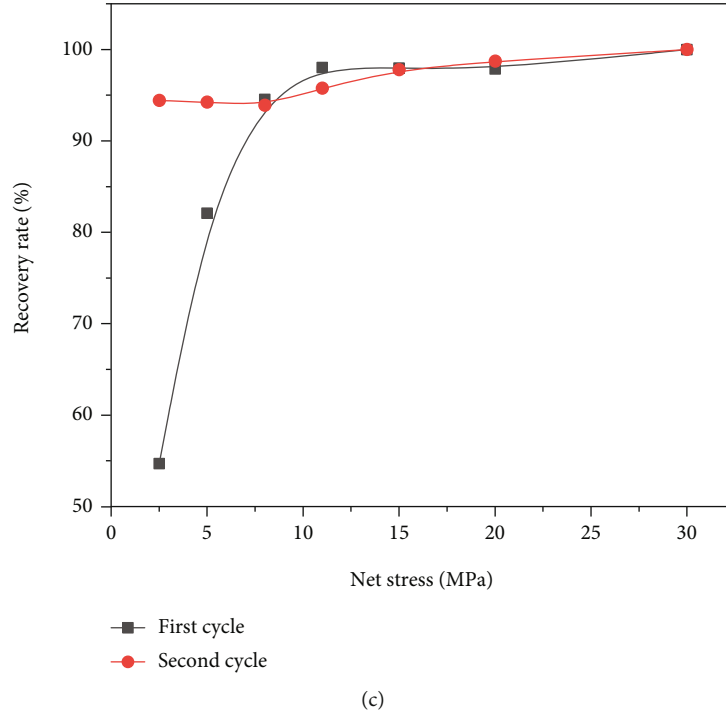
(a)
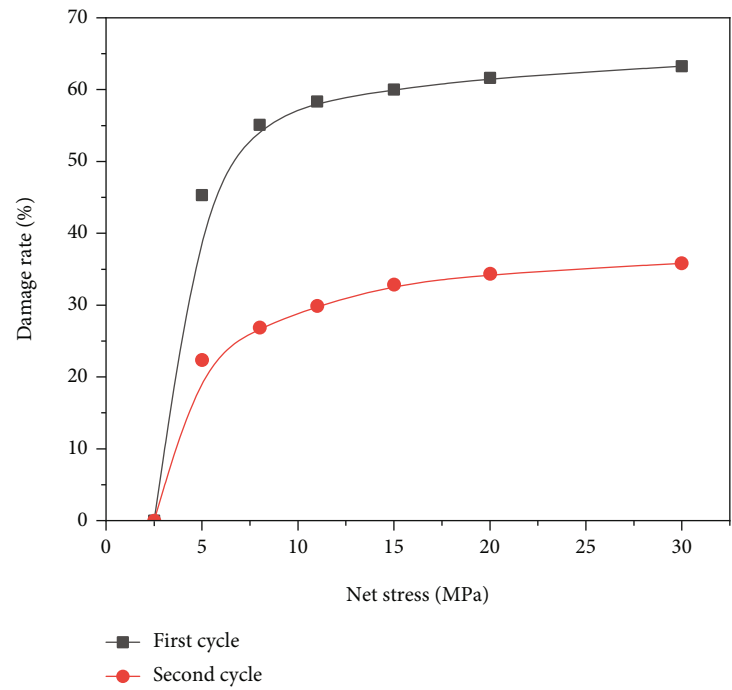
(b)

Figure 4: Continued.

(c)

FIGURE 4: (a) The relation between dimensionless permeability and net stress; (b) permeability damage rate during cyclic loading; (c) permeability recovery rate during cyclic loading.
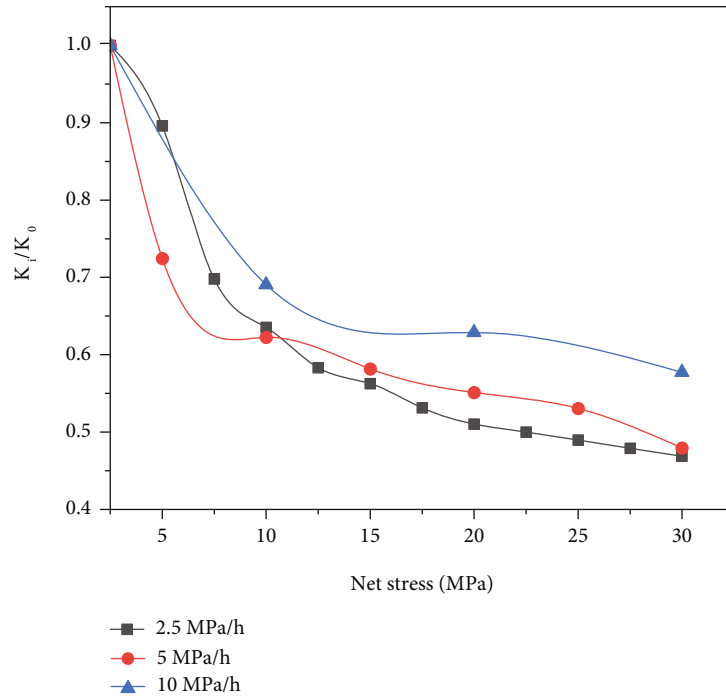

FIGURE 5: The relation between permeability and the net stress under different loading rate.

sizes and total pore volume can be obtained. Then, the variation law of pore microstructures and the corresponding relationship with permeability can be analyzed.

As shown in Figure 6, the T_2 spectrum of the core used in this study presents a double-peak structure, and the relaxation times corresponding to the peaks are 1.2 ms and
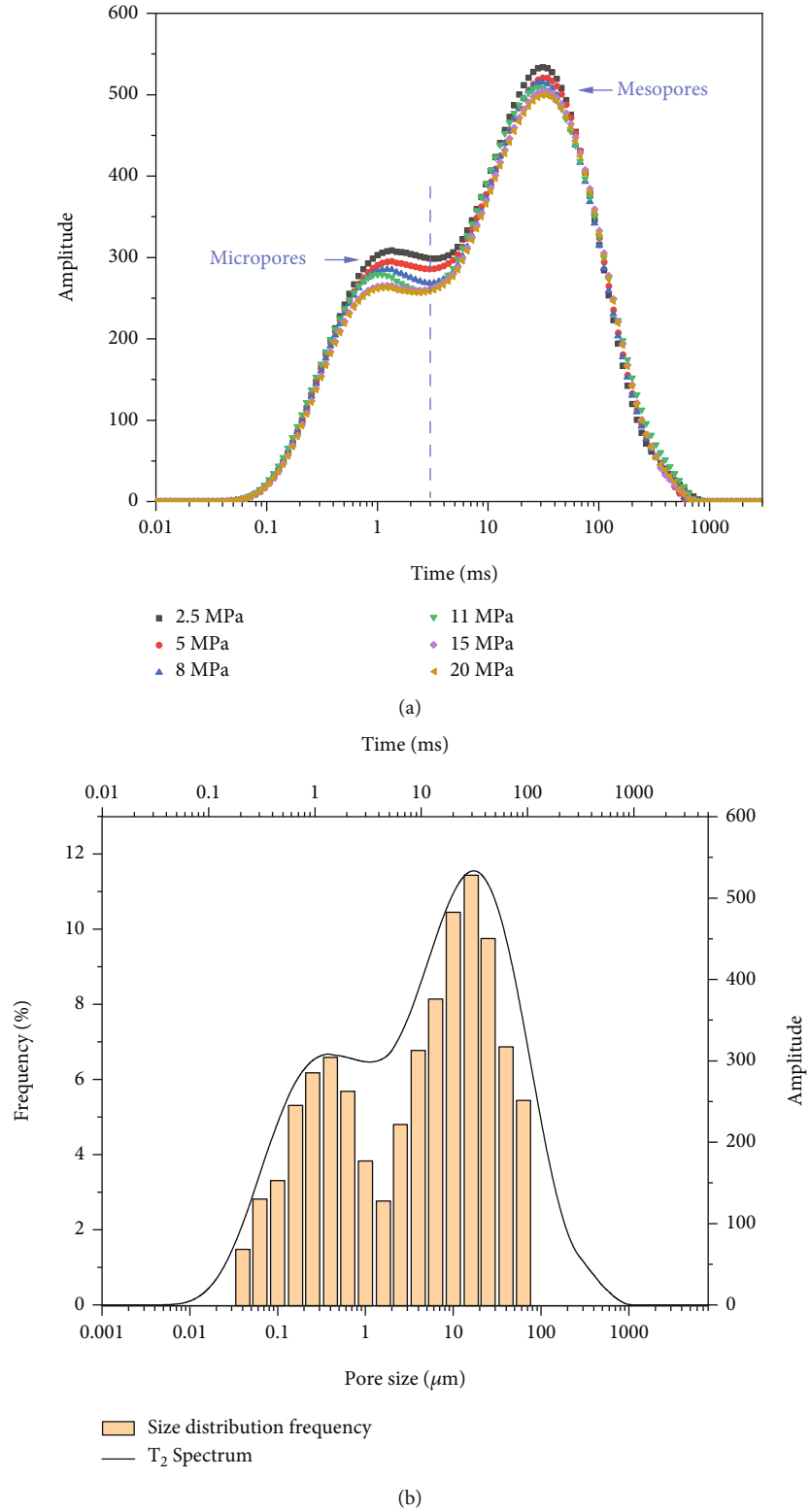
(a)

(b)

FIGURE 6: (a) A typical T_2 spectrum of the core under different net stress, (b) the coupling relation between T_2 spectrum and pore size distribution.

31.1 ms, respectively. According to the relationship between relaxation time and pore size, the core pore is divided into two parts, micropores and mesopores. Combining the T_2 spectrum with pore size distribution curve, the micropore size ranges from 0.25 to 1.6 μm, and the mesopore size ranges from 6.3 to 24.8 μm. With the increase of the net stress, the peak areas of the micropores and mesopores show a downward trend, indicating that the two types of pores
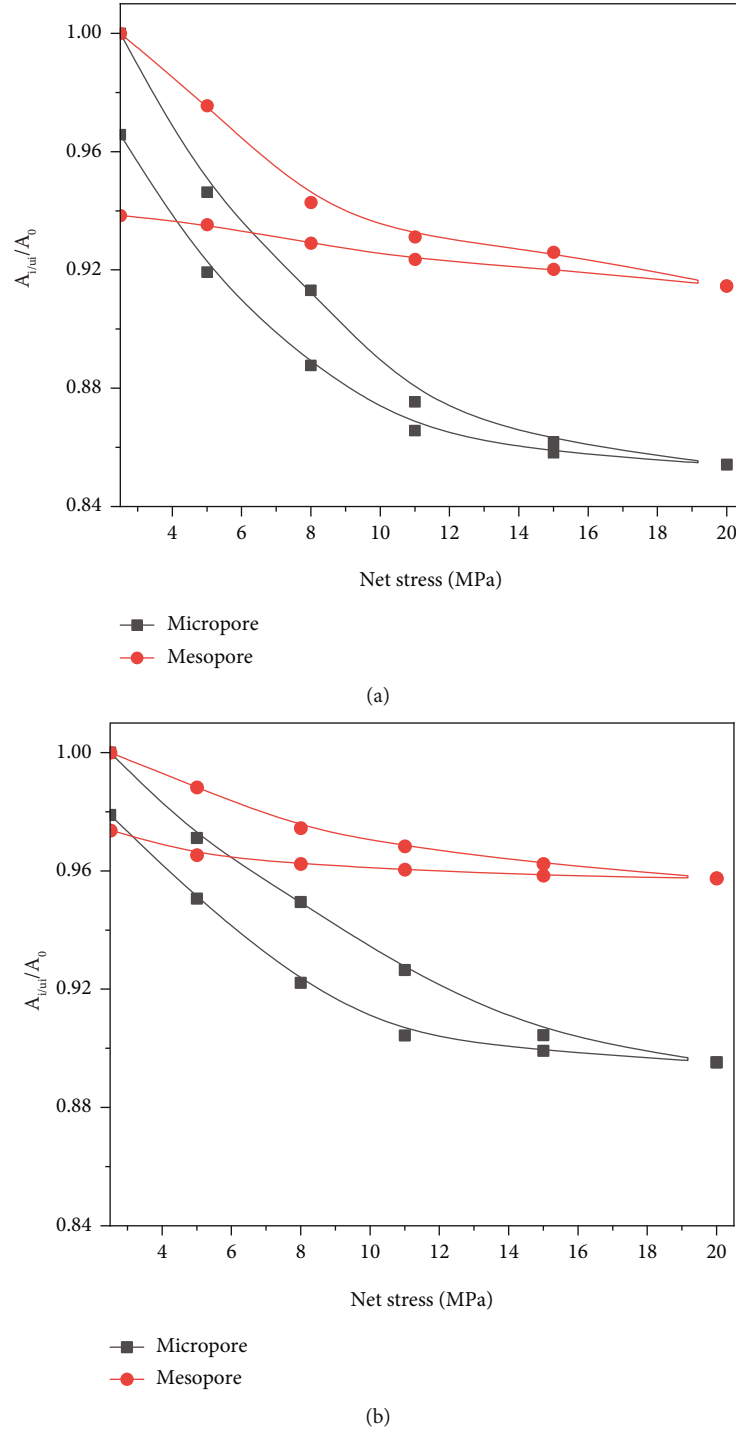
(a)

(b)

FIGURE 7: The relation between pore volume and the net stress: (a) variable confining pressure, (b) variable flow pressure.

have different degrees of shrinkage. In addition, affected by the pressure resistance of the core holder in the NMR instrument, the maximum net stress of the core in the NMR experiment is 20 MPa.

3.2.1. Loading Method. There are differences in permeability changes under the two different loading methods. This section will further analyze the variation characteristics of the internal pore structures.

Figure 7(a) demonstrates the pore volume of micropores and mesopores both present a decreasing trend with the increase of net stress under variable confining pressure loading. The damage rate of micropores (14.59%) was higher than that of mesopores (8.54%). At the same time, the recovery rate of micropores (96.6%) is also higher than that of mesopores (93.5%). It is revealed that the deformation of the rock skeleton around the micropores is mainly the bulk deformation, occurring when the stress is large and
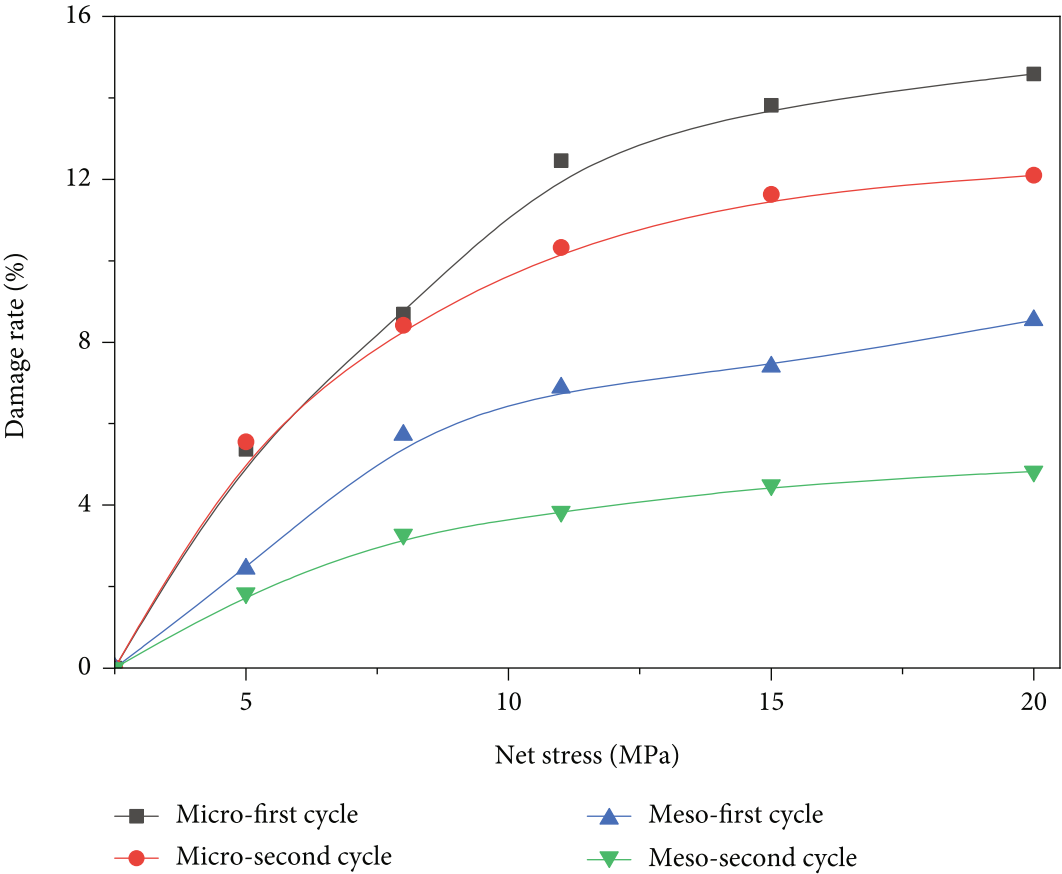
(a)
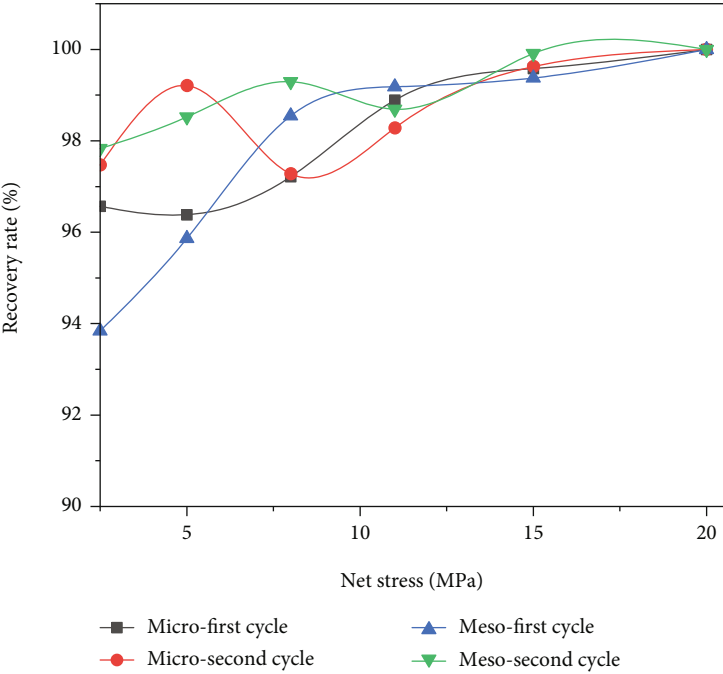
(b)

Figure 8: Damage rate and recovery rate of pore volume with different sizes under cyclic loading.
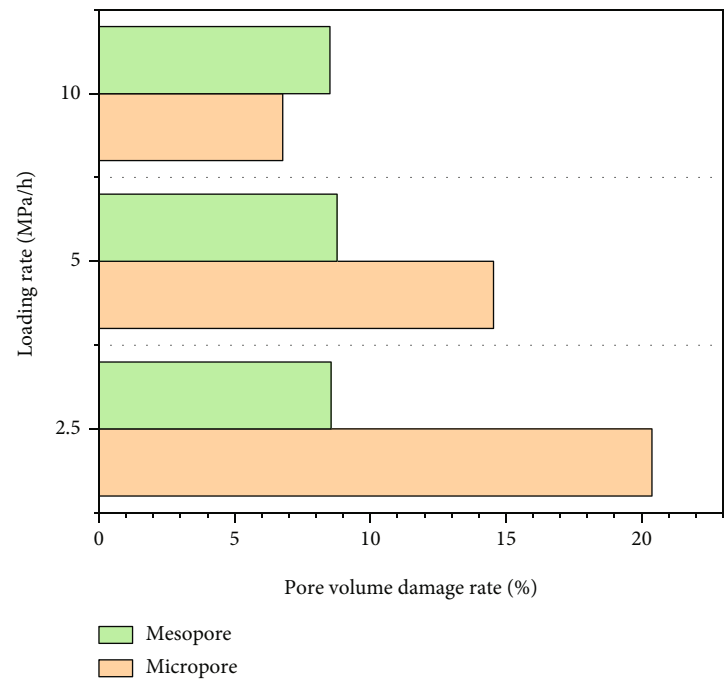
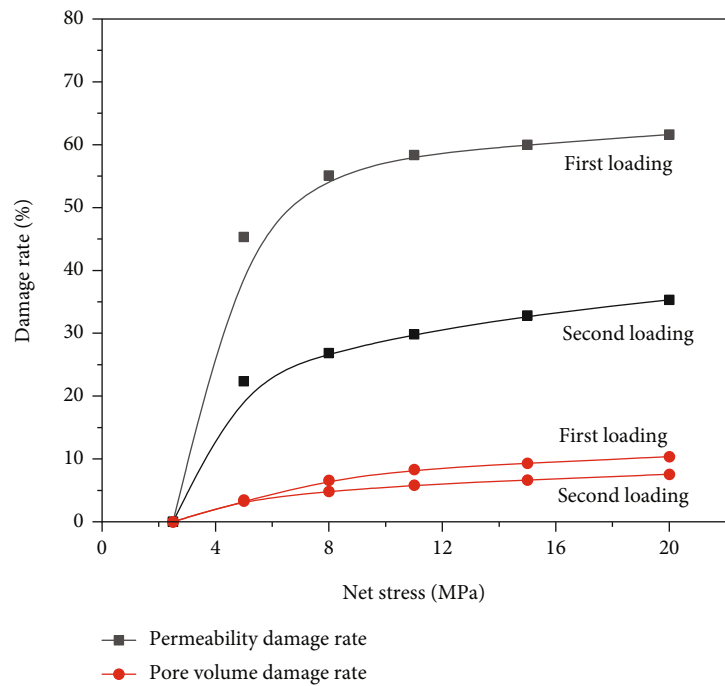FIGURE 9: Pore volume damage rate at different loading rates.

FIGURE 10: Permeability and pore volume damage rate under different net stresses.

recovering after the stress is removed. The recovery rate of mesopores is small, indicating that when the core is suddenly subjected to a large stress, the relative position and shape of the rock particles around the mesopores will change, resulting in a decrease in pore volume and irreversible recovery. As shown in Figure 7(b), the damage rate of micropores (10.5%) is significantly higher than that of mesopores (4.3%), but both are lower than the variable confining pressure test results. The recovery rate of the two is similar, and the overall recovery level is relatively high, all exceeding 97%. When the net stress changes due to flow pressure, the force application process is relatively gentle. These results
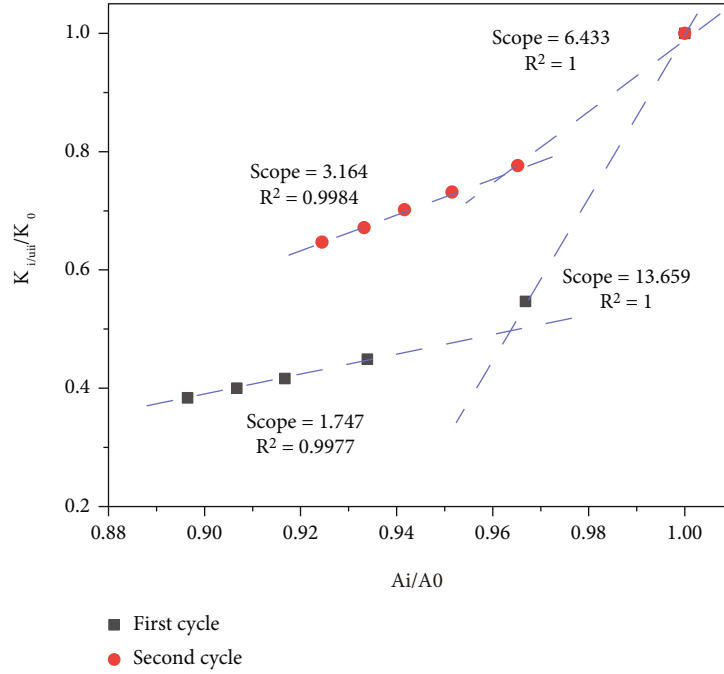
FIGURE 11: The corresponding between pore volume change and permeability.

also correspond to the permeability test results, the change of permeability under variable flow pressure is smaller than that of variable confining pressure.

3.2.2. Cyclic Loading.

The core was repeatedly loaded to count the pores volume and calculate the damage rate and recovery rate, clarifying the change characteristics of micropores and mesopores.

According to Figure 8, after cyclic loading and unloading, the damage rate shows a downward trend, with micropores dropping from 14.6% to 8.5% and mesopores from 12.1% to 4.8%. While the damage rate of micropores is always higher than that of mesopores, the damage rate rises rapidly and then gradually stabilizes. The recovery rate maintains a high level overall, especially during the second loading. The recovery rate of the mesopores is 93.5% at the first loading and the rest were more than 95%. The above content is consistent with the permeability test results. During the second compression, the overall skeleton structure is relatively stable and not prone to large plastic deformation. The rock is mainly elastic deformation and easy to recover.

3.2.3. Loading Rate.

The low-field NMR device was used to analyze the volume change characteristics of micropores and mesopores under different loading rates.

Figure 9 depicts that with the increase of loading rate, the damage rate of micropores decreases (20.4%-6.8%), an approximately linear change. Whereas the damage rate of mesopores is similar, with an average of 8.6%. It demonstrates that there are some unstable structures near the mesopores, which are easy to deform but limited in degree. The particles around the micropores are evenly and closely arranged, which has strong resistance to deformation and the sudden increase of pressure has little influence on it.

However, with the extension of loading time, the pressure conduction becomes more homogeneous and the particles are gradually compressed. Besides, when the mesopores are deformed, the surrounding cementitious substances will migrate to around micropores, which have low hardness and are easy to be compressed.

3.3. Correlation between Permeability and Pore Volume.

It can be obtained that both pore volume and permeability are damaged to varying degrees when the net stress changes. This section will further discuss the correlation between them and analyze the internal mechanism of permeability change under different net stress.

A summary of permeability and pore volume damage rate under different net stresses is shown in Figure 10. Under the same net stress, the damage rate of permeability is higher than that of the pore volume. The maximum damage rate of permeability is 63.3%, while that of the pore volume is only 10.4%. The permeability damage rate decreased significantly after repeated loading, but the pore volume damage rate remained the same for the two loadings. The cores used in this study are all dense matrix cores, in which the main mineral components are quartz and feldspar, which are difficult to compress, only slight elastic deformation occurs in most regions. The larger permeability damage rate is mainly due to the structural deformation inside the rock and the clogging of small pores by rock components such as clay minerals.

From right to left in Figure 11, the net stress increases gradually. During the first loading, the initial change of pore volume is small, while the change of permeability is large. In the later stage, the change range of pore volume increases significantly, while the change of permeability is small in the meanwhile. The slope of the fitted curve of permeability and pore volume at the initial stage of loading is ten times higher
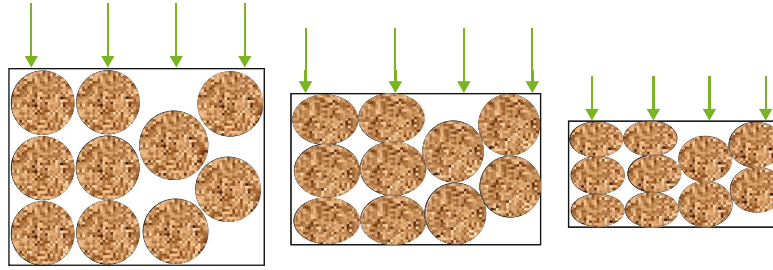
FIGURE 12: Schematic diagram of pore throat deformation.
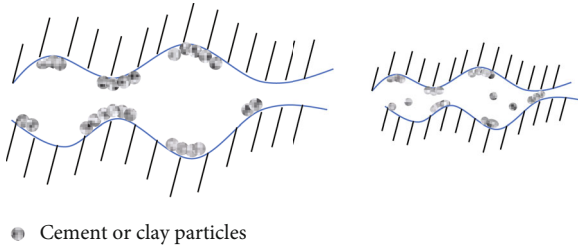

⬤ Cement or clay particles

FIGURE 13: Schematic diagram of deformation, fragmentation, and migration of cement or clay particles.

than that at the later stage of loading. During the second loading, the slopes of the fitted curves are close, implying that the permeability and pore volume maintain a relatively consistent change. After the initial loading, the pore structure of the rock is damaged and it is almost impossible to recover. During the subsequent loading process, the permeability change is mainly caused by the compression deformation of the rock particles themselves.

During the loading process, the change of rock pore structure is shown in Figure 12. Under normal circumstances, rock particles form a stable structure in different arrangements. When the external force increases, the rock particles are compressed and gradually deformed [32, 45, 46]. The contact surface between particles increases, and some of the particles slide and dislocation, which will lead to a larger decrease in permeability. Besides, clay minerals and other particles are attached to the sandstone surface [16], whose hardness is low, these particles will deform and migrate under the action of external force, blocking small pores and causing a decrease in permeability, as shown in Figure 13. As the pressure continues to increase, most of the skeleton structures tend to be stable. The compression of the rock particles leads to the reduction of the seepage space, which in turn reduces the permeability. The deformation is mostly elastic deformation, with a low degree of damage and a high degree of recovery.

4. Conclusion

In this paper, considering the stress sensitivity of tight sandstones and formation damage in the actual production process, the variation characteristics of core permeability under different stress conditions and the corresponding with pore throat microstructure were investigated by a series of physi-

cal simulations and NMR experiments. The main conclusions are as follows.

(1) As the net stress on the rock increased, its permeability decreased rapidly and then remained stable, and the net stress of the turning point is 8 MPa. The stress sensitivity of rock under variable confining pressure (63.3%) was greater than that of variable flow pressure (46.4%). Repeated loading process, the damage rate decreased (63.3%-35.8%), the recovery rate increased, and the irreversible damage to the core mainly occurred during the initial production

(2) When the net stress on the core increased, the volume damage rate and recovery rate of micropores (14.6%, 96.6%) were higher than that of the mesopores (8.5%, 93.5%), indicating that the micropores were more mainly elastic deformation and easy to recover. The plastic deformation of mesopores resulted in a decrease in permeability. After repeated loading, the micropores and mesopores were mainly elastically deformed

(3) With the increasing loading rate, the damage rate of matrix permeability decreased (53.1%-42.3%). The volume damage rate of mesopores was the same, while the damage rate of micropores gradually decreased (20.4%-6.8%). The matrix core has a stable structure, when the loading rate is fast, the force cannot be transmitted to the entire core in time, which is likely to cause local deformation. The slow loading is conducive to the uniform transmission of the force, resulting in the overall larger-scale deformation

(4) Based on the above results, in the initial stage of loading, the deformation of rock structure and the migration of cement have a great influence on permeability and it is almost impossible to recover. Later, rock particles mainly undergo bulk deformation, the contact surface between particles increasing, the seepage space shrinking, and the permeability decreasing slowly. But the compression has a certain limit, and the final permeability remains unchanged.

Data Availability

The experimental data, except the information presented in the manuscript, used to support the funding of this study is restricted by the safety law of Petrol China.

Conflicts of Interest

No conflict of financial interest exists in the submission of this manuscript, and the manuscript is approved by all authors for publication.

Acknowledgments

References

[1] Z. Caineng, R. Zhu, S. Wu et al., "Types, characteristics, genesis and prospects of conventional and unconventional hydrocarbon accumulations: taking tight oil and tight gas in China as an instance," *Acta Petrolei Sinica*, vol. 33, no. 2, pp. 173–187, 2012.

[2] X. Huang, L. Gu, S. Li, Y. Du, and Y. Liu, "Absolute adsorption of light hydrocarbons on organic-rich shale: An efficient determination method," *Fuel*, vol. 308, p. 121998, 2022.

[3] L. Yueliang, H. Jian, and C. Wang, "Absolute adsorption of CH4 on shale with the simplified local-density theory," *SPE Journal*, vol. 25, no. 1, pp. 212–225, 2020.

[4] J. Zhu, C. Fu, H. Yang et al., "Comprehensive evaluation of Chang 6 reservoir from Yanchang Formation in Ganguyi oil area, Ordos Basin," *Northwestern Geology*, vol. 52, no. 1, pp. 166–175, 2019.

[5] W. Wang, Y. Zhu, C. Yu, L. Zhao, and D. Chen, "Pore size distribution in the tight sandstone reservoir of the Ordos Basin, China and their differential origin," *Journal of Natural Gas Geoscience*, vol. 5, no. 2, pp. 45–55, 2020.

[6] Y. Liu, H. A. Li, Y. Tian, Z. Jin, and H. Deng, "Determination of the absolute adsorption/desorption isotherms of CH4 and n-C4H10 on shale from a nano-scale perspective," *Fuel*, vol. 218, pp. 67–77, 2018.

[7] Y. Jingli, D. Xiuqin, Z. Yande, H. Tianyou, C. Meijuan, and P. Jinlian, "Characteristics of tight oil in Triassic Yanchang Formation, Ordos Basin," *Petroleum Exploration and Development*, vol. 40, no. 2, pp. 150–158, 2013.

[8] X. Zhao, X. Liu, Z. Yang et al., "Experimental study on physical modeling of flow mechanism in volumetric fracturing of tight oil reservoir," *Physics of Fluids*, vol. 33, no. 10, p. 107118, 2021.

[9] S. Theerapat and N. Tutuncu Azra, "Hydraulic fracturing and production optimization in eagle ford shale using coupled geomechanics and fluid flow model," *Rock Mechanics and Rock Engineering*, vol. 50, no. 12, pp. 3361–3378, 2017.

[10] J. Wu, L. Yongren, C. Jun, and D. Lü, "A study on seepage characteristics and productivity of fractured tight reservoir Chang 3 in Weibei," *Journal of Southwest Petroleum University (Science & Technology Edition)*, vol. 43, no. 2, pp. 136–145, 2021.

[11] E. S. Mohamed, A. Kashy, and S. Ameri, "The impact of the net stress on gas recovery from the Marcellus Shale," *SPE/AAPG Eastern Regional Meeting*, 2018OnePetro, 2018.

[12] Z. W. Gao, X. F. Qu, T. J. Huang, T. Xue, and P. Cao, "Stress sensitivity analysis and optimization of horizontal well flowback system for shale oil reservoir in Ordos Basin," *Natural Gas Geoscience*, vol. 32, no. 12, pp. 1867–1873, 2021.

[13] L. Hao, Y. Zheng, J. He, and H. Zhenguo, "A new method for physical simulation of flow characteristics of fluids in shale oil reservoirs," *Acta Petrolei Sinica*, vol. 42, no. 10, pp. 1346–1356, 2021.

[14] Q. Lei, W. Xiong, J. Yuang, Y. Cui, and Y. S. Wu, "Analysis of stress sensitivity and its influence on oil production from tight reservoirs," in *Eastern regional meeting*, p. 111148, OnePetro, 2007.

[15] D. Ren, F. Yang, R. Li, Y. Li, and D. Liu, "The influential factors and characteristics of tight sandstone gas reservoir: a case study in Ordos Basin in China," *Geofluids*, vol. 2020, Article ID 6690043, 11 pages, 2020.

[16] W. L. Xiao, L. Jiang, M. Li et al., "Effect of clay minerals on the effective pressure law in clay-rich sandstones," *Journal of Natural Gas Science and Engineering*, vol. 27, no. 2, pp. 1242–1251, 2015.

[17] X. Lin, L. Xue-wei, S. Long-kan et al., "The study on experimental method of fluid stress sensitivity of low permeability in tight reservoir," *Journal of Petroleum Exploration and Production Technology*, vol. 11, no. 6, pp. 2599–2608, 2021.

[18] Z. Hu, J. Klaver, J. Schmatz et al., "Stress sensitivity of porosity and permeability of Cobourg limestone," *Engineering Geology*, vol. 273, p. 105632, 2020.

[19] Y. C. Wang, F. J. Zhou, L. F. Zhang, J. Wang, H. Y. Qu, and E. D. Yao, "Experimental investigation on stress sensitivity behavior for tight naturally fractured sandstone reservoirs," in *The 55th U.S. Rock Mechanics/Geomechanics Symposium*, Houston, Texas, USA, June 2021.

[20] M. Yingfeng, L. Chengbo, L. Gao, and L. Houbin, "An experimental study on stress sensitivity of tight sandstone gas reservoirs during nitrogen drilling," *Arabian Journal of Geosciences*, vol. 12, no. 18, p. 576, 2019.

[21] Z. Chen, L. Zheng, M. Li, W. Xiao, and Z. Liu, "The effective pressure law for permeability in northern Hubei low permeability sandstone rocks," in *The 14th World Conference on Earthquake Engineering*, Beijing, China, October 2008.

[22] M. Li, W. L. Xiao, Y. Bernabé, and J. Z. Zhao, "Nonlinear effective pressure law for permeability," *Journal of Geophysical Research-Solid Earth*, vol. 119, no. 1, pp. 302–318, 2014.

[23] Z. Jinzhou, X. Wenlian, L. Min, X. Zuping, L. Lijun, and W. Jun, "The effective pressure law for permeability of clay-rich sandstones," *Petroleum Science*, vol. 8, no. 2, pp. 194–199, 2011.

[24] Y. Xue, J. Liu, P. G. Ranjith, F. Gao, H. Xie, and J. Wang, "Changes in microstructure and mechanical properties of low-permeability coal induced by pulsating nitrogen fatigue fracturing tests," *Rock Mechanics and Rock Engineering*, vol. 55, pp. 1–10, 2022.

[25] D. O. U. Hongen, H. Zhang, Y. Shanglin et al., "Measurement and evaluation of the stress sensitivity in tight reservoirs," *Petroleum Exploration and Development*, vol. 43, no. 6, pp. 1022–1028, 2016.

[26] B. Liu, Y. Yang, J. Li, Y. Chi, J. Li, and X. Fu, "Stress sensitivity of tight reservoirs and its effect on oil saturation: a case study of Lower Cretaceous tight clastic reservoirs in the Hailar Basin, northeast China," *Journal of Petroleum Science and Engineering*, vol. 184, p. 106484, 2019.

[27] Y. Kang, C. Li, L. You, J. Li, Z. Zhang, and T. Wang, "Stress sensitivity of deep tight gas-reservoir sandstone in Tarim Basin," *Natural Gas Geoscience*, vol. 31, no. 4, pp. 532–541, 2020.

[28] S. Yin, D. Lv, and W. Ding, "New method for assessing micro-fracture stress sensitivity in tight sandstone reservoirs based on acoustic experiments," *International Journal of Geomechanics*, vol. 18, no. 4, p. 04018008, 2018.

[29] Y. Xiao, F. Shengbin, W. Jiong et al., "Stress sensitivity and its influence factors of tight oil reservoir in Chang 7 member *Ordos Basin*," *China Petroleum Exploration*, vol. 22, no. 5, pp. 64–71, 2017.

[30] H. Wang, B. Ji, C. Lv et al., "The stress sensitivity of permeability in tight oil reservoirs," *Energy Exploration & Exploitation*, vol. 37, no. 4, pp. 1364–1376, 2019.

[31] R. Deboer, "Development of porous media theories — a brief historical review," *Transport in Porous Media*, vol. 9, no. 1-2, pp. 155–164, 1992.

[32] C. Xu, C. Lin, Y. Kang, and L. You, "An experimental study on porosity and permeability stress-sensitive behavior of sandstone under hydrostatic compression: characteristics, mechanisms and controlling factors," *Rock Mechanics and Rock Engineering*, vol. 51, no. 8, pp. 2321–2338, 2018.

[33] J. Huang, F. Xiao, C. Labra, J. Sun, and X. Yin, "DEM-LBM simulation of stress-dependent absolute and relative permeabilities in porous media," *Chemical Engineering Science*, vol. 239, p. 116633, 2021.

[34] J. Shi, X. Wan, Q. Xie et al., "Difference of microfeatures among diagenetic facies in tight sandstone reservoirs of the Triassic Yanchang Formation in the Midwestern region, Ordos Basin," *Geofluids*, vol. 2021, Article ID 5611786, 11 pages, 2021.

[35] G. Liu, H. Yin, Y. Lan, S. Fei, and D. Yang, "Experimental determination of dynamic pore-throat structure characteristics in a tight gas sandstone formation with consideration of effective stress," *Marine and Petroleum Geology*, vol. 113, p. 104170, 2020.

[36] Y. Xue, P. G. Ranjith, Y. Chen, C. Cai, F. Gao, and X. Liu, "Nonlinear mechanical characteristics and damage constitutive model of coal under CO_2 adsorption during geological sequestration," *Fuel*, vol. 331, p. 125690, 2023.

[37] L. H. Bai, B. Liu, Y. J. Du et al., "Distribution characteristics and oil mobility thresholds in lacustrine shale reservoir: insights from N2 adsorption experiments on samples prior to and following hydrocarbon extraction," *Petroleum Science*, vol. 19, no. 2, pp. 486–497, 2021.

[38] H. Gao, C. Wang, J. Cao, M. He, and L. Dou, "Quantitative study on the stress sensitivity of pores in tight sandstone reservoirs of Ordos Basin using NMR technique," *Journal of Petroleum Science and Engineering*, vol. 172, pp. 401–410, 2019.

[39] F. Wang, P. Cao, Y. Wang, R. Hao, J. Meng, and J. Shang, "Combined effects of cyclic load and temperature fluctuation on the mechanical behavior of porous sandstones," *Engineering Geology*, vol. 266, p. 105466, 2020.

[40] J. Zhang, C. Wei, W. Ju et al., "Stress sensitivity characterization and heterogeneous variation of the pore-fracture system in middle-high rank coals reservoir based on NMR experiments," *Fuel*, vol. 238, pp. 331–344, 2019.

[41] H. I. Umeobi, Q. Li, L. Xu, Y. Tan, and C. C. Onyekwena, "Flow and structural analysis of sedimentary rocks by core flooding and nuclear magnetic resonance: a review," *Review of Scientific Instruments*, vol. 92, no. 7, article 071501, 2021.

[42] B. Liu, L. Bai, Y. Chi, R. Jia, X. Fu, and L. Yang, "Geochemical characterization and quantitative evaluation of shale oil reservoir by two-dimensional nuclear magnetic resonance and quantitative grain fluorescence on extract: a case study from the Qingshankou Formation in southern Songliao Basin, northeast," *Marine and Petroleum Geology*, vol. 109, pp. 561–573, 2019.

[43] X. Kong, *Advanced mechanics of flow in porous media*, Hefei: Press of University of Science and Technology of China, 2010.

[44] K. Terzaghi, "Die berechnung der curchlassigkeitziffer des tones aus dem verlauf der hydrodynamischen spannungserscheinumgen," *Sber Akad Wiss Wien*, vol. 132, no. 2, p. 105, 1923.

[45] L. Chuanliang, K. O. N. G. Xiangyan, D. Zhimin, X. Xianzhi, and L. Peichao, "Study on rheological model of porous media," *Acta Mechanica Sinica*, vol. 35, no. 2, pp. 230–234, 2003.

[46] C. Nai and L. Gang, "Stress sensitivity of tight reservoirs during pressure loading and unloading process," *Petroleum Exploration and Development*, vol. 46, no. 1, pp. 138–144, 2019.